Analysis of Quench Propagation in the ITER Poloidal Field Conductor Insert (PFCI)

Roberto Zanino, Roberto Bonifetto, and Laura Savoldi Richard

***Abstract*—We analyse the issues of quench propagation in the NbTi Poloidal Field Conductor Insert (PFCI), recently tested at JAEA Naka, Japan. The simulation tools Mithrandir, already validated against data from previous Nb3Sn Insert Coils, and M3, implementing a more detailed thermal-hydraulic description of the CICC cross section, are used. The results of the analysis are reported in the paper and compared with experimental data, with particular attention to NbTi versus Nb3Sn features and to the effects of different model assumptions.**

***Index Terms*—NbTi, nuclear fusion, quench, superconducting magnets.**

I. Introduction

THE PFCI IS A single-layer solenoid wound from a 45 m long NbTi dual channel cable-in-conduit conductor (CICC), designed to be representative of the one currently proposed for the PF1&6 coils of the International Thermonuclear Experimental Reactor (ITER) [1]. The PFCI is well instrumented from both the thermal-hydraulic point of view (thermometers glued on the jacket, flow meters, pressure taps, see Fig. 1) and the electromagnetic point of view (voltage taps, see Table I for selected locations); it was installed in the bore of the ITER Central Solenoid Model Coil at JAEA Naka, Japan [2], and successfully tested in June–August 2008 [3].

While the PFCI test concentrated on DC performance (current sharing temperature and critical current measurements) and AC loss measurements, which were recently analysed in some detail [4], a fraction of the test campaign was devoted to stability and quench propagation measurements, which were not addressed by analysis so far.

The 1-D Mithrandir code [5], already validated against stability and quench data from previous Nb3Sn Insert Coils [6]–[8] as well as against quench data from ITER sub-size conductors [9], and the quasi-3D M3 code [10], implementing a more detailed thermal-hydraulic description of the CICC cross section, are used here to analyse the issues of quench propagation in the PFCI.

II. Experimental Setup

As for the other ITER Insert Coils, stability tests of the PFCI were performed by pulsing one of the two inductive heaters (IH)

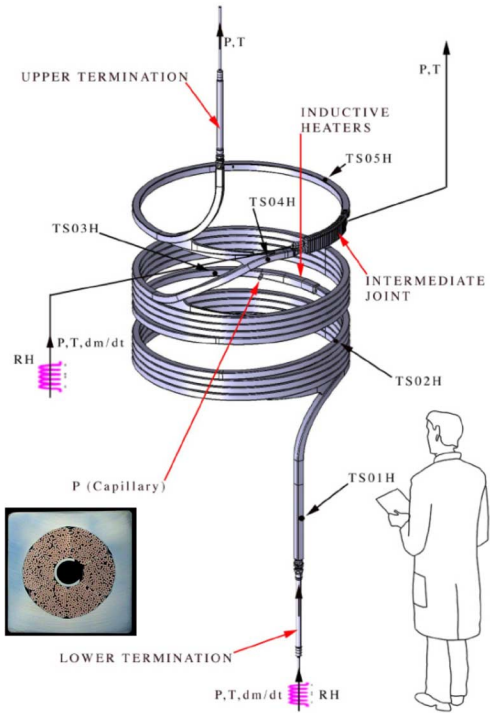

Fig. 1. Sketch of the PFCI with heaters and thermal-hydraulic diagnostics. The conductor cross section (∼50 mm side) is shown in the inset.

available near the middle of the PFCI main winding, see Fig. 2. Quench tests resulted from the repetition of the stability test with the IH set at the measured minimum quench energy (MQE), but with a sufficiently long time delay between when 0.1 V are measured along the coil and the current dump, to ensure propagation could be

Calibration tests of the IH performed at JAEA Naka, Japan, showed that, as in previous Insert Coil tests, the IH actually works mainly as a resistive heater. In the case of the PFCI ∼85% of the input energy goes to the jacket and only the remaining ∼15% directly to the strands [11]; indeed, as a confirmation of this, all of the PFCI quenches started with a considerable delay after the end of the pulse, of the order of 1 s or more, which is comparable to the heat diffusion time through the jacket thickness.

Of the five PFCI quench runs [3] we consider here run 110-07, which main features are summarized in Table II, where I is the operational current of the PFCI, B_{peak} the sum of external and self- magnetic field in the IH region, T_{in} the inlet He temperature, τ_{pulse} the heat pulse duration and t_{dump} current dump time after the pulse. observed.

Manuscript received October 22, 2009. First published March 25, 2010; current version published May 28, 2010. This work was partially financially supported by EFDA.

The authors are with Dipartimento di Energetica, Politecnico di Torino, 10129 Torino, Italy (e-mail: roberto.zanino@polito.it).

Color versions of one or more of the figures in this paper are available online at http://ieeexplore.ieee.org.

Digital Object Identifier 10.1109/TASC.2010.2041547

TABLE I
VOLTAGE TAP LOCATION

Sensor #	12	11	10	9	8	7	6	5
Location (m)	19.2	20.4	21.6	22.0	23.2	24.3	29.6	34.3

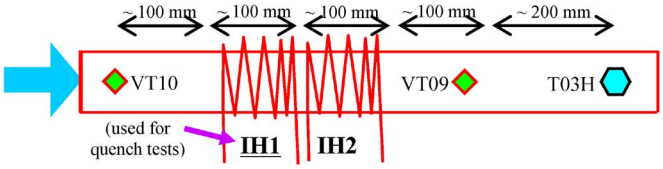

Fig. 2. Sketch of the inductive heaters region and relevant diagnostics. Helium forced flow is from left to right.

TABLE II
QUENCH CHARACTERISTICS

Run #	I (kA)	B_{peak} (T)	T_{in} (K)	τ_{pulse} (ms)	t_{dump} (s)
110-07	45	6.0	4.52	40	9.7

III. MODEL INPUT AND ASSUMPTIONS

We may distinguish three different phases in the transient we are considering:

1) External heating phase;
2) Take-off phase;
3) Quench propagation.

Phase 1 should actually require a detailed electro-magnetic/thermal-hydraulic model of the IH, as used e.g., in [6], but this is beyond the scope of the present paper. Here we parametrically studied several different space distributions of the above-mentioned 85% in the jacket (the time distribution was always assumed to be a square wave of duration $\tau_{\rm pulse}$), then following the diffusion of the heat through the jacket with a one-dimensional (radial) heat conduction model, assuming as boundary condition the jacket temperature distribution computed by Mithrandir/M3 along the length of the IH. As the heat comes to the inner surface of the jacket, it goes either directly to the strands via a thermal contact resistance with equivalent heat transfer coefficient $\rm H_{Jk-St}$, or to the He via a jacket-helium heat transfer coefficient $\rm H_{Jk-He}$ and from there to the strands via a heat transfer coefficient $\rm H_{He-St}$. Unfortunately none of these coefficients is known very well, so they are typically used as parameters to be chosen within a reasonable range by suitable parametric study. Here we use $\rm H_{St-He} = 5000\ W/m^2K$ [6], $\rm H_{Jk-St} = 500\ W/m^2K$ and $\rm H_{Jk-He} = 500\ W/m^2K$. The fourth heat transfer coefficient typically needed by 1-D code is that between central channel and cable bundle region, $\rm H_{HB}$. To estimate it we study parametrically heat slug tests performed without current during the PFCI test campaign to test the performance of the IH. The best fit of the heat slug propagation along the conductor allows the calibration of the heat transfer coefficients. An example of such a test is shown in Fig. 3: with $\rm H_{HB} = 150\ W/m^2K$ and friction factors from established correlations, a very good agreement between computed and measured temperature evolutions at the two thermometers downstream of the IH is achieved.

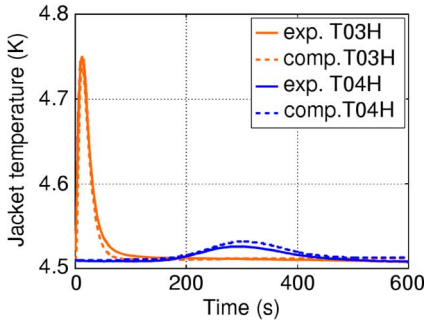

Fig. 3. Comparison between computed (dashed) and measured (solid) temperature evolutions at the two temperature sensors on the PFCI main winding downstream of the IH, during a heat slug test. T04H sensor is 21.3 m downstream of the T03H.

Phase 2 was treated so far (i.e., in the case of Nb3Sn conductors), using tools, e.g., Mithrandir, which did not distinguish details in the cable cross section, attributing to all strands in a given cross section the same temperature, magnetic field distribution etc. However, in the case of NbTi the higher sensitivity of the critical parameters to the variation of the magnetic field was demonstrated experimentally in the case of full-size ITER conductors with significant magnetic field variation on the cross section [12]. Therefore, it may be expected that M3 will be more suitable than Mithrandir for the analysis of this phase, because each petal can be described by a different temperature and He flow, sees its own field, etc..

In phase 3, where non-uniformities on the cable cross section are likely to be less important because the whole transport current flows in the Cu, the main global features of the quench, i.e., the local and overall voltage evolution and the hot spot temperature will be analysed with Mithrandir.

The PFCI coil and conductor parameters are given in [3] and the critical strand parameters in [13].

IV. RESULTS AND DISCUSSION

A. External Heating Phase

We have tried several different recipes for the distribution of the IH energy in the jacket, as well as several combinations of heat transfer coefficients. Nonetheless, the apparently inadequate IH model leads to computed MQE which are typically 2.5–5 times the measured value. In the case of a very short heating one could easily estimate an enthalpy margin as the energy needed to raise the He in the cable bundle region below the IH to $\rm T_{CS}$. In our case, however, the effective heating duration is long, because of its predominantly resistive nature (see above), therefore a simple estimate of the enthalpy margin is not achievable because the transit time below the IH and the coupling time between bundle region and central channel may be comparable with the effective heating time.

The overestimate of the MQE, however, should not compromise the calculation beyond the moment where the generated Joule energy overcomes the external input energy (which occurs for voltages ~1–2 mV), except of course the take-off time shall be anticipated. Therefore, the results for the take-off and propagation phases presented below have been shifted in order to match the take-off time.

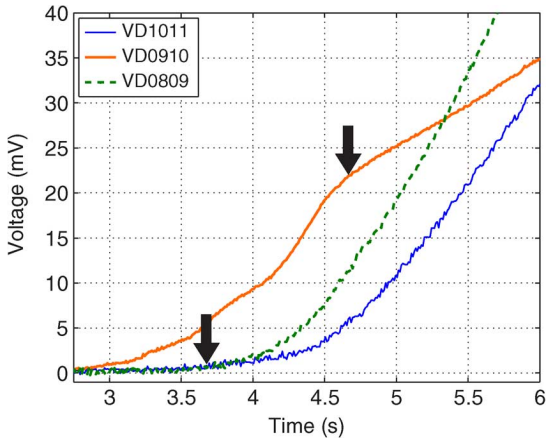

Fig. 4. Evolution of different measured local voltages in the take-off phase.

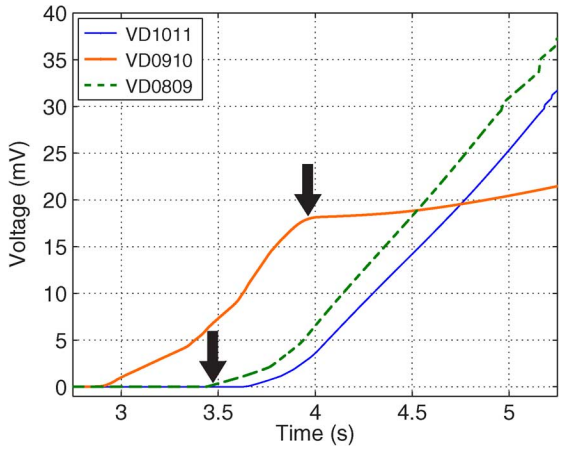

Fig. 6. Evolution of different computed local voltages in the take-off phase.

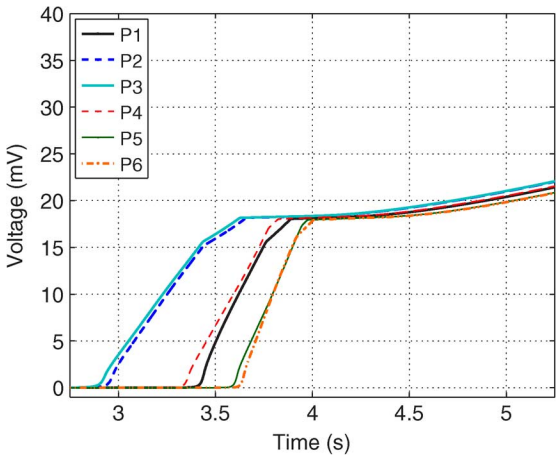

Fig. 5. Evolution of computed petal voltages over the VD0910 length during take-off.

B. Take-Off Phase

The take-off of the local voltage signals shows a very peculiar feature in the PFCI: in Nb3Sn conductors the voltage signal from neighboring regions to the IH (e.g., the VD0809 and VD1011 of Table I) takes off only when a "knee" appears in the voltage across the IH, indicating the normal zone has reached the boundary of VD0910, see Fig. 2, from which moment the voltage grows slower because it responds only to a temperature increase and no more to propagation of the normal zone; as opposed to that, in the case of the PFCI VD0809 and VD1011 take off before VD0910 shows the characteristic knee, see Fig. 4. To explain this "contradiction", it was suggested in [3] that the initial propagation of the quench could be inhomogeneous in the cable cross section.

The take-off is then studied using the M3 model, assuming uniform current distribution because of already high voltage levels (several thousand times the critical value), indicating the current will all flow in the Cu.

Because of the field gradient on the cross section, the petals do not all go normal at the same time, but rather progressively, starting with the most loaded one, see Fig. 5. If we now look at the *average* petal voltage evolution, we see that also the computed VD0809 and VD1011 take off before the VD0910 knee, see Fig. 6, as it was observed in the experiment, see Fig. 4.

Looking with the code inside the conductor cross section, see Fig. 5, it is seen that as soon as the quench in the most loaded *petal* reaches the boundary of the VD0910 region the adjacent voltage region takes off (i.e., VD0809 in correspondence of the first knee of P2/P3 at $\mathrm{t} \sim 3.4\,\mathrm{s}$, and VD1011 in correspondence of the second knee of P2/P3 at $\mathrm{t} \sim 3.6\,\mathrm{s}$). This confirms the speculation that in the NbTi CICC the initial propagation of the quench might indeed be inhomogeneous on the cross section.

Note however that, while this qualitative feature is nicely reproduced by the model, the slope after the knee is underestimated (this issue shall be addressed in the next Section). The slope before the knee, somewhat overestimated, is related to the delay in take-off of the least loaded petal with respect to the most loaded one. As such it will be related to the rate at which each petal is heated by the IH, which we know is not accurately reproduced in our model.

We see in Fig. 5 that Phase 3 is starting from $t \sim 4\,\mathrm{s}$, when the voltages computed on each petal are approximately uniform on the cross section.

C. Quench Propagation Phase

The propagation of the quench was measured using the voltage taps located at different positions along the conductor. This is compared with the computed quench propagation in Fig. 7, showing that the model accurately simulates the propagation.

The computed overall voltage evolution until the current dump is presented in Fig. 8, showing good agreement with the measurement except in the last phase of the transient where the measured voltage starts being progressively underestimated. Since a likely cause for this (as well as for the previously noted underestimation of the slope of the local voltages after the knee) could be an underestimate of the strand temperature, we should need an experimental reference for this quantity.

Since only the jacket temperature was measured in the PFCI as usual for these CICCs, there is no direct measurement of the strand temperature which can be only indirectly obtained from the measured VD0910 signal, which can be considered fully relevant of the *cable* voltage at these voltage levels, taking into

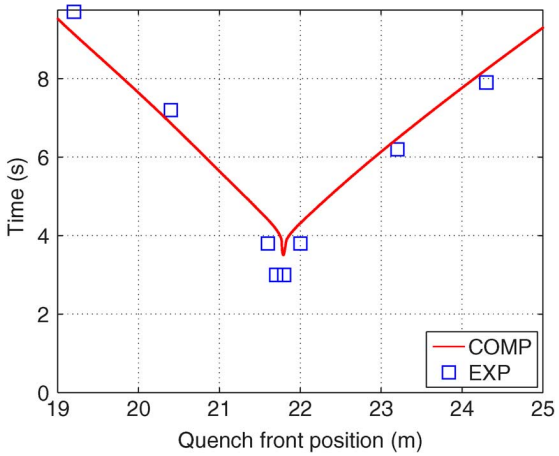

Fig. 7. Quench front propagation along the PFCI main winding. Computed (solid line) versus measured (squares).

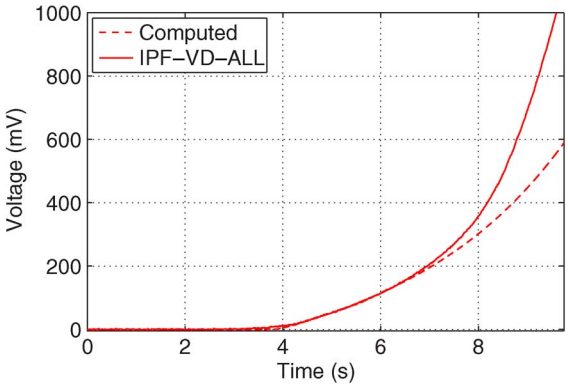

Fig. 8. Overall voltage evolution along the PFCI main winding. Computed (dashed) versus measured (solid).

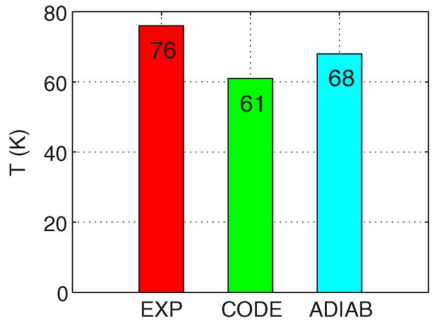

Fig. 9. Peak (hot spot) strand temperatures just before the current dump. From left to right: measured (from virtual thermometer), computed by the Mithrandir code, and adiabatic estimate.

account the temperature dependence of the Cu resistivity and assuming the temperature between the voltage taps is uniform and the whole current flows in the Cu (so-called virtual thermometer).

The virtual thermometer reading just before the dump is compared in Fig. 9 with the peak computed strand temperature, showing that the code underestimates the virtual (hot spot) temperature by $\sim$15 K. In order to try and understand this rather large disagreement in a quantity, which is usually thought to be easily estimated, as it mainly depends on the available heat capacities in the system, we also show in Fig. 9 the temperature estimate $\mathrm{T_{ad}}$ assuming an adiabatic evolution of the cable, subject to the measured Joule heating $(\mathrm{VD0910} * \mathrm{I})$ in the Cu. It is seen however that $\mathrm{T_{ad}}$ is lower than the virtual thermometer (which is a bit surprising, as the adiabatic assumption should result in an upper bound for the temperature) but higher than the peak temperature computed by the code. The reasons for this apparent contradiction and disagreement are still under investigation. Coherently with the temperature underestimation, also the pressurization is underestimated by the code (by $\sim$12%).

V. Conclusions and Perspective

The simulation of quench propagation in NbTi ITER full-size conductors is made more delicate and difficult than in the case of Nb3Sn by the increased sensitivity to gradients (field, temperature, ...) on the conductor cross-section. Indeed, it was shown that only a quasi-3D model including these gradients can reproduce the qualitative details of the take-off, including initial propagation at the petal level.

The subsequent propagation of the quench is well reproduced by the simulation using more traditional 1-D models, except in this case the hot spot temperature (with related voltage before the dump) and peak pressurization, which are somewhat underestimated by the codes at present.

Acknowledgment

RZ and LSR thank JAEA Naka, Japan, for kind hospitality during the PFCI test.

References

[1] W. Baker *et al.*, "Manufacture of the Poloidal Field Conductor Insert Coil (PFCI)," *Fusion Eng. Des.*, vol. 82, pp. 1567–1573, 2007.
[2] Y. Nunoya *et al.*, Installation and Test Programme of the ITER Poloidal Field Conductor Insert (PFCI) in the ITER Test Facility at JAEA Naka.
[3] D. Bessette *et al.*, "Test results from the PF conductor Insert Coil and implications for the ITER PF system," in *Proc. ASC '08*.
[4] R. Zanino *et al.*, "EU contribution to the test and analysis of the ITER poloidal field conductor insert and the central solenoid model coil," *Supercond. Sci. Technol.*, vol. 22, p. 085006, 2009, (11pp).
[5] R. Zanino, S. DePalo, and L. Bottura, "A two-fluid code for the thermohydraulic transient analysis of CICC superconducting magnets," *J. Fus. Energy*, vol. 14, pp. 25–40, 1995.
[6] R. Zanino, E. Carpaneto, A. Portone, E. Salpietro, and L. Savoldi, "Inductively driven transients in the CS Insert Coil (I): Heater calibration and conductor stability tests and analysis," *Adv. Cryo. Eng.*, vol. 47, pp. 415–422, 2002.
[7] L. Savoldi, E. Salpietro, and R. Zanino, "Inductively driven transients in the CS Insert Coil (II): Quench tests and analysis," *Adv. Cryo. Eng.*, vol. 47, pp. 423–430, 2002.
[8] L. S. Richard, A. Portone, and R. Zanino, "Tests and analysis of quench propagation in the ITER toroidal field conductor insert," *IEEE Trans. Appl. Supercond.*, vol. 13, pp. 1412–1415, 2003.
[9] R. Zanino, L. Bottura, and C. Marinucci, "A comparison between 1- and 2-fluid simulations of the QUELL conductor," *IEEE Trans. Appl. Supercond.*, vol. 7, pp. 493–496, 1997.
[10] L. S. Richard, M. Bagnasco, and R. Zanino, "Multi-solid Multi-channel Mithrandir (M3) code for thermal-hydraulic modelling of ITER cable-in-conduit superconductor," *Fus. Eng. Des.*, vol. 82, pp. 1607–1613, 2007.
[11] Evaluation of Inductive Heating Energy of PF Insert Coil Conductor by Calorimetric Method 2008, JAEA Internal Report.
[12] P. Bruzzone *et al.*, "Test results of the ITER PF insert conductor short sample in SULTAN," *IEEE Trans. Appl. Supercond.*, vol. 15, pp. 1351–1354, 2005.
[13] R. Zanino *et al.*, "Preparation of the ITER Poloidal Field Conductor Insert (PFCI) test," *IEEE Trans. Appl. Supercond.*, vol. 15, pp. 1346–1350, 2005.